Luis Montoto

Digital Multi-Image Analysis: Application to the Quantification of Rock Microfractography

The microfissuration of a rock sample is analyzed using a multi-image formed of micrographs which were obtained under fluorescence and polarizing microscopy of the same sample area. Image analysis methods are applied to obtain descriptions of each type of picture, one showing the microfissure network and the other the texture of the rock. Descriptions in the form of tables of coordinates are used to quantify the features contained in the pictures. Finally, it is shown that relationships between these descriptions can result in the integration of the available information, providing more knowledge about microfissuration in the sample, including characterization and quantification of microcrack types according to their position with respect to the texture of the rock.

1. Introduction

The correct discrimination and quantification of some basic petrographic parameters, such as fractography, texture, and mineralogy, are fundamental to understanding the physical properties of rock materials. In rock mechanics, the prediction of *in situ* physical properties from models of rock microcracks is an open question [1]. Applications of such information range from earthquake prediction and the exploitation of oil and gas to the storage of heat and the disposal of nuclear waste.

Despite the importance of the micromechanics of rock deformation, quantitative analysis of crack patterns is conducted today by manual methods. The discrimination of a microfissure network can be a tedious and difficult task, even with the aid of analog image processing systems in which the microscope is connected to a black and white television monitor and discrimination is accomplished by means of brightness and contrast control on the TV screen. Quantification of a microfissure network is also done manually based on arbitrary definitions of crack length and width [2]. Thus, crack surface area is estimated using photo-mosaics formed by scanning electron microscope (SEM) micrographs and counting the number of crack intersections with a test array placed at different orientations [3]. Another method uses a protractor and a simple scale to measure on the screen of a SEM the length and width of cracks that intersect a reference line drawn on the screen while the sample is traversed in a direction parallel to the line [2]. Furthermore, these time-consuming methods produce results that cannot be quantitatively comparable [3]. Thus an automated approach in which microcrack networks could be easily discriminated and geometrically quantified seemed desirable. To this end, we concluded that digital image analysis methods might be used, as had been done with different types of images [4, 5]. The author could find no other references in the literature relating to the problem of microfissure quantification by means of digital image analysis.

The discrimination and quantification of a fissure network in a rock sample does not solve the problem. The possibilities raised by the use of the different microscopy methods available today to map different types of petrographic parameters merely constitute pieces of isolated information to be put together by the geologist when he is faced with a practical situation. To clarify this point, we consider as an example the problem of storing radioactive waste in rock caverns [6]. Here, one needs to quantify the microfissure network developed in granitic rock specimens when they are subjected to different in situ heating conditions. But that information is not enough to predict, for example, the future behavior of the rock unless other parameters, such as the texture of the rock, are quantitatively related to microfissu-

© Copyright 1982 by International Business Machines Corporation. Copying in printed form for private use is permitted without payment of royalty provided that (1) each reproduction is done without alteration and (2) the *Journal* reference and IBM copyright notice are included on the first page. The title and abstract, but no other portions, of this paper may be copied or distributed royalty free without further permission by computer-based and other information-service systems. Permission to *republish* any other portion of this paper must be obtained from the Editor.

ration. Thus, of special importance in the study of rock microfractography is the characertization of fissure positions with respect to the texture of the rock: intra-, inter-, and transgranular fissures, depending on whether they are located inside grains or between grains, or run through different rock-forming minerals. Additionally, the geologist would like to know what percentage of the total length of fissures runs between grains of type A, what fissures are inside grains of type B, or what the grain size distribution is for the different mineral species. With the methods available today, these types of questions about relationships between fissures and grains can only be answered in a qualitative way [3].

Thus, the most valuable and complete information is obtained when, first, different microscopic methods (fluorescence, polarizing, acoustical, electron, etc.) are applied to the same area in the sample, so that basic petrographic parameters are mapped into different pictures with similar resolutions; second, the petrographic features in each picture are described by digital analysis methods; and, third, the descriptions are correlated in order to integrate all the available information, providing a complete description of the sample, including quantitative values. This approach can provide deeper insight into the problem being considered.

We call the procedure just outlined the multi-image analysis approach. The term multi-image, as used here, refers to the set of different pictures or micrographs obtained by the application of different microscopic techniques to the same area in the specimen. This method is applicable to other areas of science to study a given scene or object that can be mapped into several pictures, each picture highlighting very different aspects of the original scene.

It is interesting that, regardless of the sophistication of the techniques available today to obtain multi-images (from satellite pictures to micrographs) and the increasing number of digital image analysis methods used to describe the contents of a picture, there appears to be little corresponding effort to extract the information available in a multi-image set.

Multi-image sets of two or three pictures were considered recently, although no image analysis methods were applied to describe the original scene. In one case, each picture in the set was inspected visually to obtain some qualitative information about the scene [7, 8]. In the other case the pictures were combined (after registration when needed) by feeding them to separate guns of a color TV monitor, thus creating a color composite picture that could be better interpreted visually than any one of its parts [9]. In other cases, the composite picture was created by calculating ratios between the original pictures in the multi-image [10].

Multi-band images from earth resources satellites are simple examples of multi-images, since pictures in the set are not very different in terms of regions and their shapes. In fact, multi-band images were created for field classification purposes [11]. Thus, in the context of multi-image analysis, field classification has been the only application so far.

In our case, multi-image analysis originated from the need to detect grain boundaries in rock samples using polarizing microscopy, which is the most appropriate technique in petrographic studies. However, regardless of whether neighboring mineral grains in a sample are the same or not, they can exhibit under crossed polarizers the same interference color. This gives rise to significant errors in properly delimiting grain borders when only one polarizing microscope picture is used [12, 13].

In the following section of the paper we consider the digital multi-image approach. The microfissuration of a rock sample is analyzed using digital methods. This involves the following steps: first, a new method of quantifying the microfissure network is presented in detail; second, the texture of the rock is analyzed; and third, the multi-image approach presented in this paper is applied to the analysis of the rock sample in order to relate in a quantitative way the network of microfissures to the texture. Finally, a section is devoted to hardware and software considerations. Some conclusions are then drawn about the new methods presented and their possible application to other areas of science.

2. Digital multi-image analysis

Multi-image analysis is merely an extrapolation of the descriptive process that is presently applied to the contents of a single picture to the descriptive process of a real object that is instead mapped into several pictures. To achieve a more complete description of the object mapped into the multiimage, one needs descriptions of each picture in the multiimage set. Then, by properly relating these descriptions, properties of the original object can be revealed that were not apparent in the original pictures. To more easily relate descriptions from different pictures, digital image analysis methods are applied to each picture in the set by performing the following steps after picture digitization: segmentation into regions, region description, and extraction of descriptions. In this way, all of the information originally contained in raster form is "vectorized." Final descriptions for each picture are in the form of tables of coordinates, so that any property of the objects contained in the pictures can be easily calculated. Also, relationships among objects within each picture or among different pictures can be handled by manipulating the tables of coordinates. This approach has proved to be successful when dealing with the quantification of pictured objects. In fact, since descriptions of objects present in a picture can be obtained from their line drawing representations, it seems natural to extract such descriptions as lists of coordinates of their lines or lists of vertices from their polynomial approximations.

Knowledge of the specific techniques used to obtain each picture making up the multi-image allows the user to guide the different processing techniques required to analyze the individual pictures in the multi-image.

Picture registration is the extra computational work that must be done when dealing with multi-images. However, knowledge of how the image was formed can help in obtaining the transformation polynomial without the need of using control points. This is particularly useful when using a computer-driven microscope that uses different techniques to map a given sample.

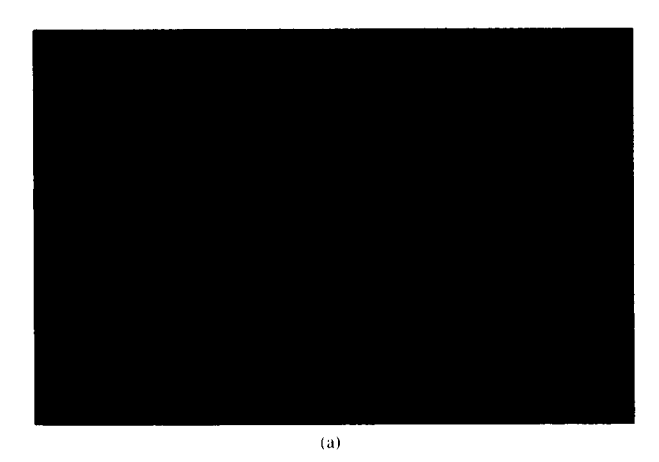
3. Analysis of rock microfissuration

The quantification of rock microfissuration is treated here as an example of a problem where multi-image analysis methods can give definitive information.

The problem of sample preparation is not a trivial one if the multi-image is going to have mapped into its different pictures the different petrographic aspects of the sample under study. It is especially important to avoid the introduction of artifacts during sample preparation. Here, and following [6], because of the type of rock studied, the problem addressed, and the sample preparation method used, microfractographic artifacts can be considered to be smaller than $10 \mu m$, and microfissures smaller than $100 \mu m$ in length were not evaluated. The ion thinning technique was not used. By using fluorescein-impregnated, gold-metallized, thin (30 μ m thick) polished sections of rock samples, different optic and electron microscopy methods can be applied to the same area of the sample, and texture, mineralogy, state of alteration, and fractography can be mapped into different pictures. For simplicity, we consider such a sample observed under (1) light-reflected fluorescence microscopy [Fig. 1(a)], where only the microcrack network is observed, and (2) polarizing microscopy with crossed polarizers [Fig. 1(b)], where the mineralogy and texture of the rock are apparent. To solve the problem of rock microfractography, objects in the multiimage of Fig. 1 should be described by applying image analysis methods, and the relationships between those descriptions should answer questions about the incidence of cracks in the grains of the rock.

• Image digitization

Images recorded on 35-mm film are digitized with a flat-bed microdensitometer (Perkin-Elmer PDS M1010A). To meet the Nyquist criterion [14], the sampling interval to digitize an image is taken as W/2 in the x and y directions, where W is the side of the square sampling window used and is



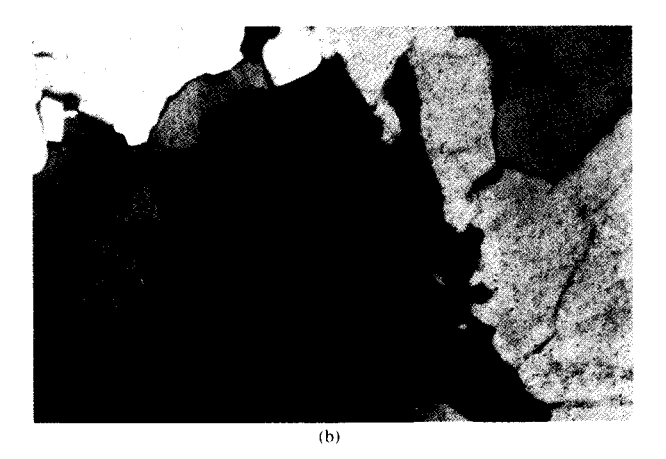


Figure 1 Different optic microscopy techniques applied to the same area of a medium heated Stripa granite (130°C) to relate the rock microfractography to its texture and mineralogy. (a) Light-reflected fluorescence microscopy; (b) Polarizing microscopy with crossed polarizers. Longest side of pictures is 2.7 mm. The set forms a multi-image of two pictures.

measured in length units relative to the film. Then, the resolution R of the digital image depends on microscope magnification, photographic enlargement, and on the W value, and is given by the product $W \times s$, where s is the dimensionless scaling factor between sample and film (i.e., the ratio between the corresponding linear measure in the sample and in the film).

The two micrographs of Fig. 1 were chosen such that the longest side of the negatives, 35 mm, covers 2.72 mm on the sample so that s=0.0777 (magnification is 1/s=13), and the digitization process was done using $w=100~\mu\text{m}$, so that resolution is $R=7.8~\mu\text{m}$. Pixel size is $7.8\times7.8~\mu\text{m}$ and pixel values are coded into 8 bits (a range from 0 to 255). Image size is usually 460×700 pixels.

• Image registration

Image to image registration is done to relate the digital images resulting from the pictures in Fig. 1. To this end a

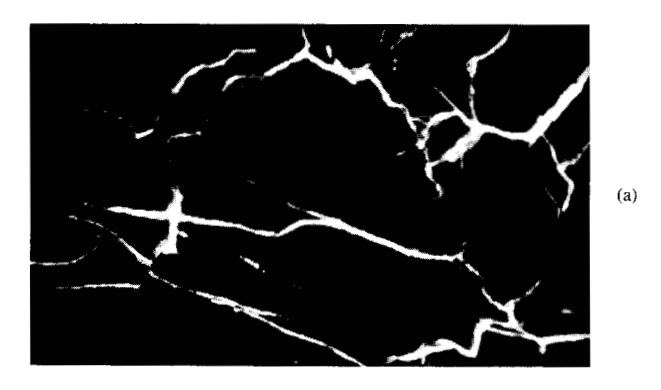




Figure 2 A digital multi-image resulting from the one in Fig. 1. The picture 2(b) is registered to that in 2(a). Resolution is 7.8 μ m.

spatial transformation algorithm builds a pair of second order bivariate polynomials using 15 control points (pixels) scattered throughout the image. The selection of control points and matching in both images were done visually on the screen of a display system. The estimated standard deviation of the errors in the position of the control points was 1.07 and 1.19 pixels in the x and y directions, respectively. Finally, resampling was done using the nearest-neighbor technique. The resulting digital images can be seen in Fig. 2, where images (a) and (b) are now registered to each other.

Work is in progress to connect the microscope used to obtain the pictures in Fig. 1 to an IBM Series/1 computer, so that digitization can be done with a TV camera attached to the microscope. Then, changing the microscope technique (light-reflected fluorescence or polarizing) will result in the corresponding digital images of Fig. 1. These images are then registered to each other by a mere translation required by the different optical paths of the two microscope techniques.

• Analysis of the fissure network

Segmentation into regions The use of fluorescence microscopy to observe a fluorescein-impregnated rock sample is the

preferred enhancement process to record the object of interest, namely, the fissure network. Other (petrographic) aspects of the sample, such as mineralogy, do not appear in the picture. Thus, in this case the segmentation process is reduced to simple thresholding, which can be done while the original micrograph is being digitized. To this end one only needs to properly set the offset and gain of the microdensitometer's photomultiplier to produce a digital image, Fig. 2(a), where all the background and noise "sinks" into the zero gray level (black in the figure). This digital image is not a binary one, but the original picture has been segmented into two regions: the fissure objects (with elongated or tree-like shapes and pixel values greater than zero) and the background.

The next step in the analysis is to describe those elongated regions by their medial lines, which are obtained through a thinning transform. It is well known [15] that noisy boundaries of an object give rise to lateral branches (artifacts) in the medial line output of the thinning transform. For this reason these boundaries of the fissure objects should be smoothed out. Thus a "field-cleaning" algorithm is applied to the digital picture in Fig. 2(a). The algorithm assigns the central pixel of a window of a given size (3×3) in this case to the class fissure-object if the number of pixels of this class inside the window is greater than the number of pixels belonging to the class background. The result is a binary image, Fig. 3, where objects with areas less than a given threshold value have been erased as well. It should be noted that this algorithm can also erase fissures one or two pixels wide (up to 16 μ m). Should this be of importance, the resolution of the original digital image should be increased by reducing the sampling window (or increasing the magnification factor of the microscope).

Description of regions As already stated, elongated or tree-like objects such as the fissure network can be described by a thinning transform. The transform used [16] reduces every object to its medial line, given as a set of curves one pixel wide, without losing the connectivity of the object. As an extra result, pixel values at the coordinates (i, j) of the medial line are equal to the fissure width at the corresponding (i, j) positions. Moreover, the set of coordinates (i, j) representing the medial line are digital curves coded in the eight-way form (that is, every pixel of the medial line could have neighbor pixels in any of the eight allowed positions in the digital image).

The output after applying the thinning transform to the picture in Fig. 3 is the digital image in Fig. 4 (where for printing purposes the medial line pixels (i, j) have been assigned the same gray level). Let S be the total area covered by the objects to be thinned (and evaluated by counting the pixels in every object), and let w(i, j) be the object's width at

(i, j) after the thinning has been done. The error of the algorithm can be evaluated by the expression

$$E = \frac{S - \Sigma w(i, j)}{S},\tag{1}$$

where the sum is extended to all elements in the medial line. This error arises mainly from the width values w assigned by the algorithm to the medial line pixels located at end branches. Thus, it does not affect the calculation of the medial line length.

The resulting E value when a thinning transform is applied to the fissure object in Fig. 4 is E=5.9%, the mean width of the object is $w=49.1~\mu m$ (6.3 pixels), and its elongatedness (or length/width ratio) is S/w=337.4. These values are used to stop any further processing if they are beyond an established range, so that interactivity between the user and the image system is not required.

From the w(i, j) values, a histogram of width values and the densities of objects of a given width can be calculated if desired.

Extraction of descriptions To calculate the lengths and directions of the fissure network, represented by the lines in the picture of Fig. 4, an omnidirectional line-following algorithm [17] is applied to this picture. The output is a set of tables of coordinates of ordered pixels belonging to the lines in the input picture. The algorithm scans the input image row by row until a pixel value different from zero is encountered. That pixel belongs to a line that the algorithm starts to follow. When the line and all its branches have been followed (and their coordinates registered in the table), the algorithm returns to the start pixel in the line and continues to scan the picture until another line, or the bottom right pixel in the image, is encountered. Inputs to the algorithm are

- 1. Maximum gap over which to jump to follow a broken line (3 pixels in this case.).
- 2. Option to record lateral branches of up to 2 pixels long (option = no: these lateral branches could be artifacts of the thinning process, due to noise in the object's boundary; thus, because the mean width of the fissures is 6.3 pixels, and taking into account the magnification used in the microscope, these lateral branches have no significance from the point of view of rock fissuration.)
- 3. Elimination of lines n pixels long from the final list (n = 3).
- 4. Pixel size in metric units.

By condition (3) 51 lines (with a total of 85 pixels) were eliminated and another 50 were left. Note that by allowing the algorithm to jump over up to 3 pixels, the 85 pixels eliminated should be noise in the input image. The number of lines and pixels eliminated acts as a warning for the quality



Figure 3 Binary image from Fig. 2(a) with the fissure network.

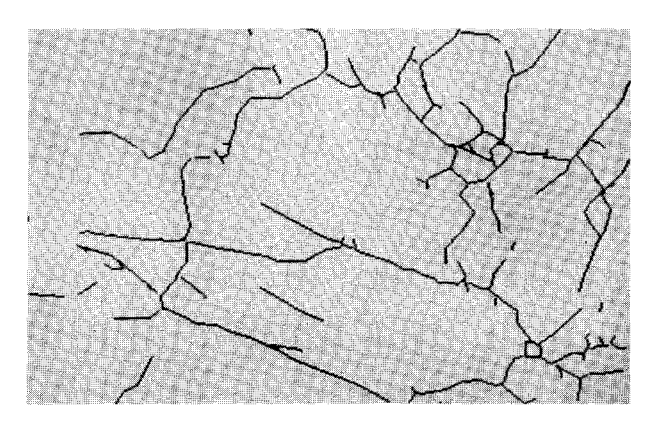


Figure 4 Description by thinning of the fissure network in the image of Fig. 3.

of the processing done up to this point. In fact, analysis of fissure networks could be done without monitoring the resulting digital images.

Quantification The lines followed were situated on a square grid (the sampling grid) and were represented in the eight-way code. Thus, the distance between two neighbor points in the line and their relative directions are quantized to 1 or $\sqrt{2}$ pixel length units (strictly speaking, this is the 8 $\sqrt{2}$ -way code in the sense of [18]) and to 0°, 45°, 90°, and 135°. With this encoding scheme the total length of the 50 lines left in the image is 20.35 mm.

If we assume that the measured curved lines are constituted of small segments of successive tangents to that curve, the total length l of the fissure network is affected by an average relative error of

$$e = \frac{l(\text{calculated}) - l(\text{true})}{l(\text{true})},$$
 (2)

739

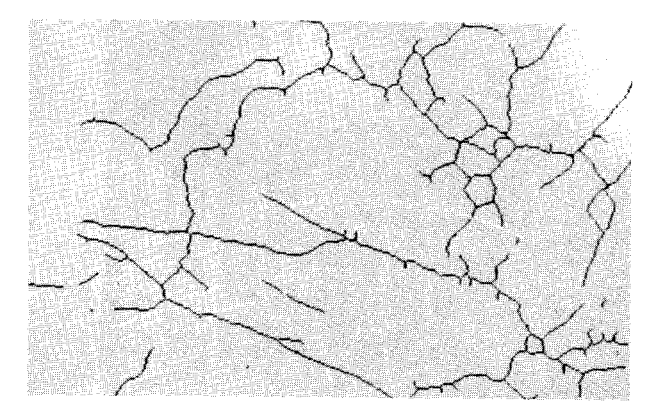


Figure 5 Vector image produced from the table of vertices of the approximated polygons to the lines contained in the image of Fig. 4.

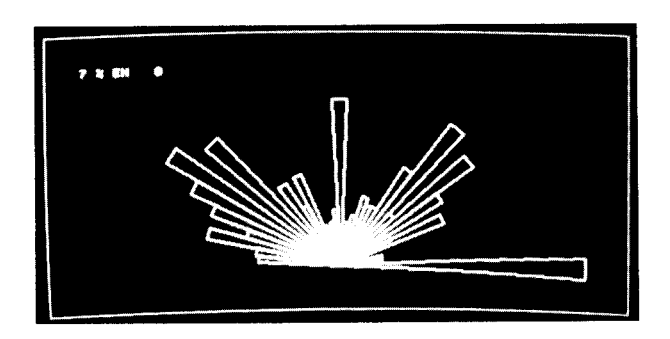


Figure 6 Direction histogram in intervals of 5° corresponding to the polygons in Fig. 5. As indicated, 7% of the line's total length is at 0° direction, which results in the most populated one.

which for the encoding scheme used is e = 5.5% [18]. (The average is related to the orientation of the small segments or straight lines measured.)

To get rid of the quantization in direction and thus to calculate the length of the fissures along any given direction, the lines represented by the final table of coordinates are approximated by polygons that are accurate within a given tolerance [19], resulting in a table of the pixel's coordinates of the polygon's vertices. The vertices of the polygonal approximation were chosen from the points in the original list in such a way that they are as far apart as possible, while the maximum distance between the polygon and the approximated arc stays within some pre-established approximation threshold p, measured in pixels.

The table of coordinates of the polygon's vertices is the final result of the digital processing applied to the original

input image. This table is also the source used to compute any description (length, shape, etc.) of the object mapped in the original picture. Moreover, the table can be used to reconstruct the fissure network (Figs. 5 and 9) as a vector image or to calculate an orientation histogram of the network (Fig. 6). In both examples an approximation threshold p=1 pixel was used.

The main advantage of the polygonal approximation (besides that of reducing stored data) is the elimination of the four quantized directions in the original line. However, its use raises the question of what approximation threshold p should be used. An orientation histogram done with a large value for p (p greater than 5 pixels) enhances the main directions contained in the fissure network, but, in turn, decreases the calculated value for the fissure's total length. On the other hand, making p = 0 pixels (which does not mean that the approximation has not been done) gives for straight lines oriented precisely at 0°, 45°, 90°, or 135° a calculated length with error e = 0 (this is the limiting situation in the m-sampling of [18], where every mth point in the line is selected to construct segments from which the length of the line is calculated). However, for other straight lines and curves, the p = 0 pixels approximation raises the cited error to e = 5.5% in the calculated length. The orientation histogram calculated from the p = 0 pixels case reflects the encoding scheme used, so directions are along 0°, 45°, 90°, and 135° only.

To find a compromise value for p, the problem is stated in the opposite way. Given a pair of points P_s and P_f on a digital image, find the list of eight-connected points that make up the straight line P_sP_s . For every new point to be interpolated between P_s and P_f there are three possibilities if the final list is eight-connected (in fact, only two need be considered in the implementation), and the choice will be that point, P_i , out of the three that gives a minimum distance d_i between P_i and the straight line $P_s P_t$. If one calculates the maximum value of all d_i encountered when creating lines $P_i P_i$ of length greater than, say, 10-15 pixels and along all directions between 0° and 45°, the result is 0.49 pixels. Thus, approximating by polygons an eight-connected digital curve (or straight line) using an approximating threshold of p = 0.49 pixels will result in polygons having the longest side that still results in the optimum length and directions for the approximated arc.

It is interesting to try to relate the approximation threshold p to the error e in the calculated length values. In eight-connected straight lines with no approximation being considered, the error is e=5.5%, as was stated. Certainly this error will be the same if one calculates the length values doing an approximation of p=0 pixels (this is not correct if in the image there are only straight lines oriented precisely at

the four main directions considered in a digital image). So one is tempted to look for that p value that yields the true length value and e=0 (i.e., the length obtained using no approximation and corrected for 5.5% in excess). When using different typical images like the one in Fig. 4, one finds that to get e=0, the p values should be near p=0.6 pixels, which is very close to the p=0.49-pixel value mentioned in the last paragraph.

The approximated polygons could also be used to calculate the number of their intersections with square grid of a given size, yielding a result that is often associated with a density of fissuration.

Results The calculated total length of the fissure network coded in the eight-way scheme is 20.35 mm. If the network is approximated by polygons, with p=0.49 pixels, the total length is l=19.70 mm with an error of e=2.1%, estimated by extrapolating the value e=5.5% when the length is calculated without approximation.

• Analysis of the texture (granulometry)

Segmentation into regions Segmentation of digital images showing rock texture could be done by the usual thresholding techniques [20]. If different and neighboring grains in the sample exhibit the same interference color under polarizing microscopy, grain boundary detection will fail unless the microscopist rotates the sample with respect to the crossed polarizers until each grain is properly mapped (the alternative [12, 13] is to use different images, as was mentioned in the Introduction). In Fig. 2(b), segmentation was done using a median filter in the space domain. Then, to the output values of the filter a threshold selection was applied based on the gray level histogram of the original digital image [13]. Next, the "field-cleaning" algorithm explained above and used now with a 5×5 window was applied to the resulting digital image. The output is the digital image of Fig. 7, where small areas, arising from noise in the original picture, disappear, and the vanished pixels are ascribed to the grains where they are located.

Description of regions The regions located in the picture of Fig. 7 are described naturally by their boundaries. Boundary detection is a simple task in this image: Boundary points are those pixels whose four four-way neighbors do not have the same gray level (or which do not belong to the same region). The output is a digital image (Fig. 8) where each region has its own boundary line; that is, region *i* has all its boundary pixels with gray value equal to *i*. Also, boundary lines are eight-way encoded. The regions (grains) in the figure have been labeled for reference.

Extraction of descriptions The line-following algorithm applied to the picture in Fig. 8 produces the tables of coordinates of grain boundaries. While scanning the digital



Figure 7 Digital image resulting from segmenting into regions the image in Fig. 2(b).

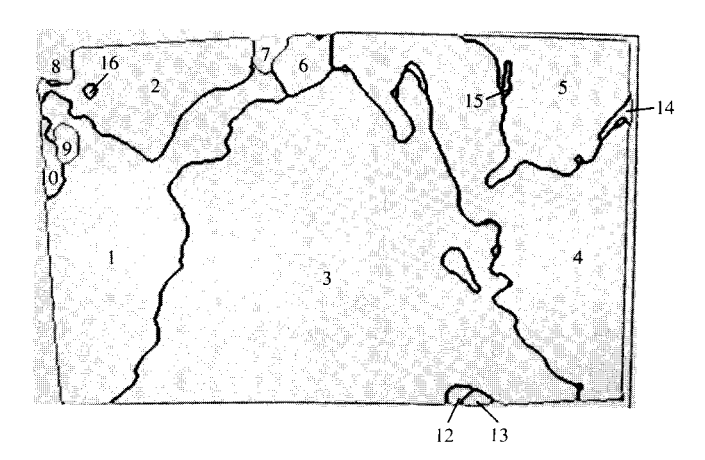


Figure 8 Boundary description of the regions (grains) in the image of Fig. 7. The grains are labeled for reference.

image, the algorithm follows lines of constant pixel values (unlike the case of the fissure lines). As boundary lines are closed, the maximum jump allowed by the algorithm is one pixel (with the result that boundary lines get smoothed). Also, final lists of lines with 10 pixels or fewer are eliminated, since they surely came from small regions due to noise.

Quantification Lists of coordinate points belonging to boundary lines represented in eight-way code allow the computation of final values describing the grains in the original picture of Fig. 2(b). Those lists have been further reduced in size by using a polygonal approximation with p=0.49 pixels. From these lists the primary image parameters can be computed, such as perimeter P, area A (from the Gauss formula, [21]), centroid coordinates, etc., and derived parameters such as dispersiveness of a region given by the dimensionless quantity $P^2/4\pi A$ (with a lower bound of one, measured in the real plane, when the object has the most



Figure 9 Graphical relationship between information from the two pictures in the multi-image of Fig. 2.



Figure 11 Fissures contained in grain no. 3, from which a fissuration density is calculated. Only one intragranular fissure of length 0.33 mm is visible in the center of the lower part of the grain; all other fissures are portions of transgranular ones.

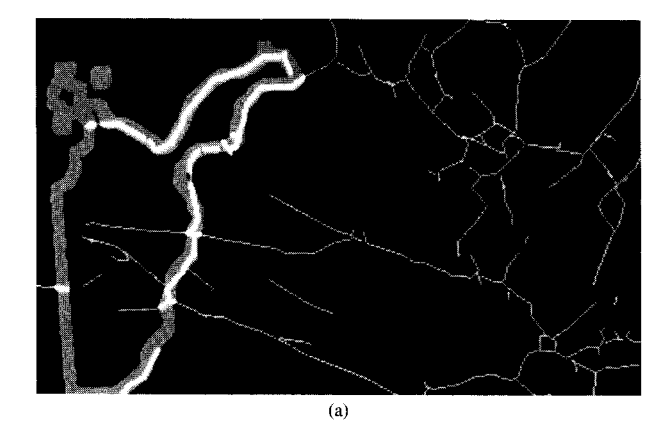




Figure 10 The problem of localization of intergranular fissures with grain no. 1: (a) representation; (b) solution. See text for details.

compact possible shape), shape factors, and other features for grain characterization [22]. Of special importance is the quantification of those boundaries that are common to two different classes of grains or to one specific class (for example, find the percentage of the total boundary length of grains of class A that are in contact with grains of class B). This problem is treated in the next section.

Results Table 1 presents under the heading of "grains" some characteristic values of the grains labeled in Fig. 8. Dispersiveness factors were determined from the original values of P and A as calculated by the computer, and not from the rounded ones that appear in the table.

• Analysis of the rock sample

In the preceding sections, features contained in the two images of Fig. 2 were analyzed separately, without considering any relationships among the contents of the images. Certainly more information about the rock sample could be gained if descriptions from the two pictures were related, as one would do visually by inspecting the picture of Fig. 9, where the fissure network has been displayed on top of the classified grains. Of special importance, as was mentioned in the Introduction, is, for example, the characterization of the fissures according to their positions with respect to the texture of the rock. To solve this problem (and the one stated above about grain boundary contacts), one has at hand tables with the coordinates of vertices of planar open polygonal lines (fissures) and closed polygons (grains). Thus the problem is reduced to the manipulation of these tables.

A set of algorithms has been developed for polygon manipulation [23]. Of special importance for the purpose stated in this section is the following: Given two polygons, one either open or closed and the other closed, find the coordinates of crossing points and common points, and label other points with inside-outside flags. In all cases, outputs of

Table 1 Numerical results of granulometric and fractographical analysis. Observed area for fissures: 4.89 mm²; observed area for grains: 4.46 mm²(*); total length for fissures: 19.70 mm.

Grains						Fissures					
Grain no.†	Perimeter P (mm)	Area A (mm²)	Dispersive- ness P ² /4π A	Covered area (%)	Intragranulars		Intergranulars		Transgranulars		density (Fi + Fi)/A (mm-1)
					$F_i(mm)$	(%)	$F_b(mm)$	(%)	$F_i(mm)$	(%)	` ,
1	5.76	0.69	3.83	15.5	0.10	0.5	3.03	15.4	1.20	6.1	1.88
2	2.81	0.30	2.13	6.7	0.00		1.04	5.3	0.00		0.00
3	7.69	2.01	2.34	45.1	0.33	1.7	5.33	27.6	4.05	20.6	2.18
4	7.28	0.90	4.72	20.2	0.08	0.4	4.22	21.4	2.82	14.3	3.22
5	3.26	0.32	2.64	7.2	0.00		1.90	9.6	0.32	1.6	1.00
6	0.98	0.056	1.35	1.3	0.00	_	0.69	3.5	0.00		0.00
7	0.54	0.017	1.39	0.4	0.00		0.12	0.6	0.00	_	0.00
8	0.54	0.019	1.22	0.4	0.00	_	0.00	_	0.00		0.00
9	0.47	0.013	1.38	0.3	0.00		0.02	0.1	0.00	_	0.00
10	0.87	0.019	3.14	0.4	0.00		0.00	_	0.00		0.00
11	0.57	0.013	2.01	_0.3	0.00		0.33	1.7	0.00	_	0.00

^{*}See Fig. 2

the algorithms are tables of coordinates (in fact, pointers to the input tables of coordinates) from which further quantification of new features can be computed.

Nevertheless, the problem of finding intergranular fissures, *i.e.*, the ones common to boundary grains, could not be resolved by this polygon manipulation. The reason is that if one attempts to find points common to both fissure lines and boundary lines from different, though registered, digital images, the probability of coincidence of points from both lines, even when they do visually coincide, is very low. For the same reason, parts of fissures that visually run along boundary lines can be misclassified as being internal to a grain.

This problem could be handled as follows: (1) Create a rectangle for every segment of the approximated boundary line given; the segment would be the longest medial axis of that rectangle, so that a closed polygon would be created for every segment; (2) Find the fissure lines that are inside the closed polygons that represent the grain boundary. This solution takes too much computing time, so the solution actually implemented is based on the same idea, but it is easier to implement and faster in execution time:

- 1. From the original list of coordinates of the given boundary, create a strip s pixels wide, such that the grain boundary is its medial line; and
- 2. From the original list of coordinates of the fissures, create a new list with the fissure points that are in the strip.

As for the value s, a strip 5 or 7 pixels wide is sufficient to compensate for the combined errors in the registration

process, the situation of the medial line in the thinning transform, and the segmentation-plus-boundary-detection algorithms, which affect the location of fissure lines and grain boundaries. Figure 10(a) shows graphically how to find the fissures that are common to boundaries of grain no. 1, and Fig. 10(b) shows a representation of the solution.

Results The fissures that originally appeared in Fig. 2(a) have been classified according to their position in relation to the grains in Fig. 2(b). The following parameters have been considered for each grain, and their values are listed in Table 1 under the heading "fissures":

- 1. Intragranular fissures: length and percent of the total length of the fissure network, exhibited by fissures which start and end in the interior of the grain.
- 2. Intergranular fissures: as in (1) for portions of fissures that run along the boundary of the grain.
- 3. Transgranular fissures: as in (1) for portions of fissures inside the grain and that run through different grains.
- 4. Density of fissuration: calculated from the ratio of length of fissures located inside the grain to grain area.

In point (4), the fissures located in the grain are the intragranular ones plus those portions of the transgranular fissures that are located inside the grain. The fissures contained in grain no. 3 have been displayed in Fig. 11 as an example. Among all of the fissures, an intragranular fissure is clearly visible in the middle of the grain; that fissure is 0.33 mm in length according to Table 1. The fissuration density thus calculated assumes fissures of unit width, although actual width values are available in the original list of coordinates of the fissure lines.

[†]See Fig. 2.

4. Hardware and software

The algorithms employed in this work are written in PL/I and belong to an image analysis interactive system that has been used in remote sensing, petrology, and biology applications [13]. Once a specific problem is defined, the system helps the user to set up a working procedure to solve it, so that interactivity can be kept to a minimum or not used at all. The system, based on a Ramtek RM9351 display terminal (with color and black and white monitors and a joystick), runs under VM/CMS in an IBM 370/158 computer. Times given in this section refer to the average response time in a time sharing environment.

The analysis of micrographs produced under fluorescence microscopy containing a network of fissures has been done with no visual interaction between the user and the images at the display terminals. Numerical results from the thinning process, the most problematical of all the steps, replace the qualitative result based on visual observation. Thus, the thinning error and the mean width and elongatedness of the object (fissures) to be thinned are values used to quantify the process. Another reason to rely upon those numerical values is the long processing time taken by a thinning transform [16]. For pictures similar to the one in Fig. 3 with 500×500 pixels, it takes about 5 minutes to obtain the medial line of the objects, depending upon their thickness and area. Then, using a computer-driven microscope, it is possible to analyze the microfissuration of a sample by programming different observations (for statistical purposes), and doing all the steps of the digital analysis for each observation in an unattended manner. All other steps in the analysis (preprocessing, line following, polygonal approximation, etc.) last less than 1 minute in total. In conclusion, for each micrograph obtained under fluorescence microscopy, the analysis of the fissure network requires the time for the digitizing process (2-3) minutes with the Perkin-Elmer microdensitometer) plus about 6 minutes of processing time.

The first and most important step in the analysis of the texture of the rock using polarizing microscopy micrographs is the segmentation of the image into regions (grains). Unless a considerable amount of *a priori* knowledge about the rock texture and grain forming minerals is introduced as input to the process, interactivity should be used in this segmentation process. Nevertheless, the whole analysis is very fast, lasting less than 5 minutes, depending of the number of regions in the image.

Manipulation of polygons to obtain numerical information from both rock texture and rock microfissuration lasts about 1 minute. Obviously this time depends on the number and size of the grains and on the number, length, and position of fissures. Image to image registration is very time-consuming while one is selecting the control points in both images. Subsequent processing, such as calculation of the transforming polynomial and resampling, takes 2–3 minutes though. As was mentioned, the whole process could be speeded up if images to be registered were obtained with the same computer-driven microscope.

5. Summary and conclusions

The digital multi-image analysis approach has been applied to the analysis of the microfissuration of a rock sample. Steps to analyze different kinds of pictures of the same sample have been considered in detail. Special mention should be made of the new method presented to analyze fluorescence microscopy-produced micrographs, where the problem of object discrimination (image segmentation) is drastically reduced due to that microscopy technique. In addition the objects that are going to be quantified, the microfissures, have elongated and tree-like shapes. Finally, relationships among vectorized descriptions of objects contained in the two pictures of the multi-image considered have demonstrated their importance in the quantifying of microfissuration in relation to the texture of the rock. Human effort and computing time seem justified if one considers the already large investment in sophisticated equipment required to obtain pictures and the quantitative rather than qualitative nature of the final results.

Based on the results presented in this paper it would be worth trying to apply these methods in other areas of science where image analysis presents similar problems. For example, neuronal structures fall into the class of objects with elongated and tree-like shapes, with the main problem being how to convert these objects, visualized through a microscope, into a three-dimensional representation. The problem of object discrimination is partially resolved by special staining methods. Then, in order to try to automate the three-dimensional vectorization of the neuronal structures, digital image analysis could be applied along the lines presented here to quantify the microfissure network. As for the multi-image approach, many sophisticated techniques are available today to map a given scene or object into different pictures. Medicine, biology, materials science, and remote sensing are a few of the areas where this approach should be beneficial as well.

6. Acknowledgments

This work is one of the results of a collaborative study between the Department of Petrology (University of Oviedo, Spain) and the IBM Madrid Scientific Center with the aim of quantifying petrographic parameters of interest in the study of rock behavior. The author acknowledges the significant contribution of Prof. M. Montoto, head of that department, in developing the ideas and methods presented in this

paper. The author also wishes to thank M. Cogollos and J. L. Navalón of the IBM Madrid Scientific Center for guiding him in the use of their algorithms for the manipulation of polygons, and to F. Orti, of the same center, for his critical reading of the manuscript.

References

- 1. B. Atkinson, "Cracks in Rocks Under Stress," *Nature* 290, 632 (1981).
- R. L. Kranz, "Crack Growth and Development During Creep of Bare Granite," Int. J. Rock Mech. Min. Sci. & Geomech. Abstr. 16, 23-35 (1979).
- T.-F. Wong, "Micromechanics of Faulting in Westerly Granite," Int. J. Rock Mech. Min. Sci. & Geomech. Abstr. 19, 49-64 (1982).
- L. Montoto, M. Montoto, and A. Bel-lan, "A Method to Measure Pores and Fissures in Geologic Materials Under S.E.M. by Digital Image Processing," *Proc. 9th Int. Cong. Electron Microsc.* 1, University of Toronto, Toronto, Canada 212-213 (1978).
- M. Montoto, A. Bel-lan, and L. Montoto, "Microscopic Quantification of Textures and Fissures in Rocks by Digital Image Processing," Proc. 3rd Int. Cong. Int. Assoc. Eng. Geol., Sec. II, Vol. 2 (Servicio Geológico de O. P., Madrid), 51-60 (1978).
- M. Montoto, L. Montoto, K. Roshoff, and B. Leijon, "Microfractographic Study of Heated and Non-Heated Stripa Granite," Subsurface Space: Proc. Int. Symp. Rockstore '80, Vol. 3, M. Bergman, Ed., Pergamon Press, Inc., Elmsford, NY, 1981, pp. 1357-1368.
- G. S. Cargill III, "Electron Acoustic Microscopy of Polycrystalline Metals and Alloys," Proc. 39th Meeting Electron Microsc. Soc. Amer., Atlanta, GA, August 10-14, 1981.
- R. L. Hollis and R. Hammer, "Defect Detection for Microelectronics by Acoustic Microscopy," Scanned Image Microscopy,
 E. A. Ash, Ed., Academic Press, Inc., New York, 1980, pp.
 155-164.
- 9. M. I. Daily, T. Farr, and C. Elachi, "Geologic Interpretation from Composited Radar and Landsat Imagery," *Photo. Eng. Remote Sensing* 45, 1109-1116 (1979).
- J. Fasset and G. H. Morrison, "Digital Image Processing in Ion Microscope Analysis: Study of Crystal Structure Effects in Secondary Ion Mass Spectroscopy," Anal. Chem. 50, 1861– 1866 (1978).
- Remote Sensing: The Qualitative Approach, P. Swain and S. Davis, Eds., McGraw-Hill Book Co., Inc., New York, 1978.
- A. Bel-lan, L. Montoto, and M. Montoto, "Digital Processing of Microscope Images: Quantification of Petrographic Parameters Related to the Quality of Crystalline Stones," Proc. Int. Symp. on Deterioration and Protection of Stone Monuments, UNESCO, Paris, 1978, Sec. 5-2, pp. 1-20.

- L. Montoto, "Image Analysis Methods on Quantification of Linear Features," Proc. IBM Int. Conf. Image Processing & Pattern Recognition, IBM Research Center, San Jose, CA, 1978, pp. H3.1-7.
- W. K. Pratt, Digital Image Processing, John Wiley & Sons, Inc., New York, 1978, p. 96.
- R. Stefanelly and A. Rosenfeld, "Some Parallel Thinning Algorithms for Digital Pictures," J. ACM 18, 255-264 (1971).
- 16. A. Bel-lan and L. Montoto, "A Thinning Transform for Digital Images," Signal Proc. 3, 37-47 (1981).
- L. Montoto, "Digital Detection of Linear Features in Satellite Imagery," Proc. Int. Symp. Image Processing Interactions with Photogrammetry & Remote Sensing, Technical University, Graz, Austria, 1977, pp. 149-153.
- D. Proffitt and D. Rosen, "Metrication Errors and Coding Efficiency of Chain-Encoding Schemes for the Representation of Lines and Edges," Computer Graph. & Image Process. 10, 318-332 (1979).
- J. Jiménez and J. L. Navalón, "The Structure of Queries on Geometric Data," *Data Base Techniques for Pictorial Applica*tion, A. Blaser, Ed., Springer-Verlag New York, 1980, pp. 219-232.
- J. S. Weszka, "A Survey of Threshold Selection Techniques," Computer Graph. & Image Process. 7, 259-265 (1978).
- Z. Kulpa, "Area and Perimeter Measurement of Blobs in Discrete Binary Pictures," Computer Graph. & Image Process. 6, 434-451 (1977).
- E. E. Underwood, "Quantitative Stereology," Addison-Wesley Publishing Co., Reading, MA, 1970.
- M. Cogollos, J. L. Navalón, and J. Jiménez, "Visualization, Reconstruction and Manipulation of Three-Dimensional Objects in Two-dimensions," *Proc. 5 Cong. Informática y Automática* (in Spanish), Madrid, May 4-6, 1982, pp. 509-514.

Received March 11, 1982; revised June 24, 1982

Luis Montoto IBM Spain, Paseo de la Castellana, 4, Madrid I, Spain. In 1972 Dr. Montoto joined the Madrid Scientific Center, where he has worked in acoustic digital signal processing. Since 1974, he has been working in the area of digital image analysis in satellite and micrograph pictures. He received the equivalent of the M.Sc. in physics from the University of Barcelona in 1967 and the Ph.D. from the Autonomous University of Madrid in 1980. In collaboration with the Optics and Condensed Matter Department of the Autonomous University of Madrid, Dr. Montoto is working on switching and electroluminescence in ferroelectric crystals. Dr. Montoto is a member of the American Crystallographic Association and the American Institute of Physics.